THE JOURNAL OF PHYSICAL CHEMISTRY LETTERS
A JOURNAL OF THE AMERICAN CHEMICAL SOCIETY

pubs.acs.org/JPCL Letter

Formation of Carbon−Carbon Interlinkage Bonds under High Pressure

Qingbo Sun,* Jian-Tao Wang, Xingshuo Huang, Guoyin Shen, and Jodie E. Bradby*

Cite This: https://doi.org/10.1021/acs.jpclett.5c01578 Read Online

ACCESS | Metrics & More | Article Recommendations | Supporting Information

ABSTRACT: The formation of carbon−carbon interlinkage bonds (CCIBs) via the chemical binding of interlayer carbon atoms of many sp^2-bonded carbon precursors is an essential step for synthesizing various diamond and diamond-like materials. Although the existence of CCIBs may be reasonably assumed under high-pressure conditions, direct experimental evidence has been scarce. Micro-Raman spectroscopy is here employed to track *in situ* the evolution of C−C bonds in a pressure range from ambient to 54 GPa. A pressure-induced two-stage (polynomial and linear) shift of the G peak and new generation of the CCIB peak at about 1550 cm^{-1} are observed in multiple types of layer-structured carbon precursors, including glassy carbon, natural graphite, and carbon nanotubes. The experimental discovery of CCIBs holds significance in comprehending phase transitions of sp^2-bonded carbon materials and has implications for the advancement of novel carbon structures.

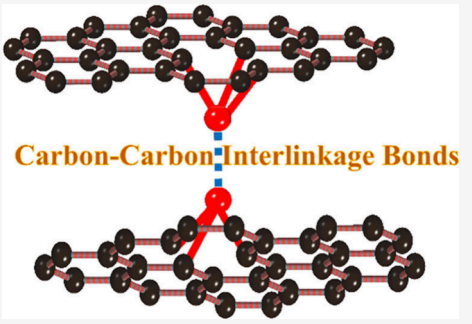

The s and p electron orbitals of carbon atoms can hybridize in the form of linear sp, triangular sp^2, and tetrahedral sp^3 covalent bonds. Such diverse C−C chemical bonds lead to various carbon allotropes, which range from a vitreous state like glassy carbon or amorphous diamond to a para-crystalline structure with short- or medium-range order but long-range disorder[1,2] to a complete crystal with a regular lattice periodicity such as graphite, cubic diamond, and Lonsdaleite. All of these abundant polymorphs and bonds give carbon materials a wide range of properties and applications. For instance, monolayer graphene is a promising material for modern electronic devices, and cubic diamond is commercially used in cutting tools due to its ultrahardness.[3−5]

To artificially synthesize various types of diamonds with variable crystallographic arrangements of C tetrahedra (i.e., amorphous, cubic, and hexagonal diamond) through using carbon precursors such as graphite and glassy carbon,[5,6] the phase transition of sp^2- to sp^3-bonded carbon has been intensively investigated for many decades. The energy barrier to form sp^3 bonds from sp^2 bonds is up to 0.33 eV per C atom[7−9] (this value depends on a specific reaction pathway,[10] selected precursor, and other factors like internal defects) and is too high to conquer without an extremely high pressure and even a simultaneous high temperature. Previous work under high pressure generated in diamond anvil cells (DACs) found that both ∼100 GPa and a high shear force were required to form cubic and hexagonal diamond from sp^2-bonded glassy carbon.[6,11,12] At an intermediate pressure of ∼45 GPa and a shear force, glassy carbon underwent a structural rearrangement at room temperature, but its reaction products retrieved after depressurization were still mainly composed of sp^2 bonds and had no evidence of the formation of recovered sp^3 bonds.[13,14] Other researchers also observed that the sp^2 to sp^3 bond transition could not be realized at an intermediate pressure such as ∼49 GPa[15] or ∼60 GPa[16] but required an extremely high pressure of ∼93 GPa[17] or ∼113 GPa[18] at room temperature. The pressure for the sp^2 to sp^3 bond transition can be significantly decreased by the combination of a high temperature, for instance, to ∼18 GPa at 1850−2000 °C[19] for preparing nanocrystalline cubic diamond and to ∼30 GPa at 950−1350 °C[1] for synthesizing para-crystalline sp^3-bonded carbon composites. Although these excellent explorations clearly indicate that sp^2-bonded carbon precursors can change to sp^3-bonded ones under suitable reaction conditions, it is not well understood how sp^2 bonds become sp^3 bonds and how sp^2 phases evolve to sp^3 phases.

In order to understand the specific changes of C−C chemical bonds and the detailed processes of the phase transition of carbon materials under high-pressure conditions, an *in situ* synchrotron X-ray diffractometer and an *in situ* X-ray absorption spectrometer have both been used.[17,20−23] However, the experimental results are still unclear given the weak X-ray scattering of carbon atoms, the restriction of achievable pressure values, and specimen sizes in DACs at a high pressure like above 50 GPa. The pair distribution function of glassy carbon indicates that interlinkages of carbon atoms between

Received: May 24, 2025
Revised: June 21, 2025
Accepted: June 24, 2025

turbostatic graphene layers could possibly occur within a pressure range of up to 49 GPa, but they are not in the form of tetrahedral sp^3 bonds.[15] Under compression, carbon atoms that have higher energy due to thermal fluctuation or defective structures may initiate to chemically bind with those from neighboring layers until finally forming perfect tetrahedral sp^3 bonds.[24−26] This assumption about the generation of carbon−carbon interlinkage bonds (CCIBs) under high pressure is reasonable in light of simple physical reasoning but currently lacks direct experimental evidence.

Raman spectroscopy is a powerful tool to analyze the bond vibration features and structural information about carbon materials under *in situ* high-pressure conditions.[16,18,27−31] It has the advantage of being a laboratory-based technique and so is more easily accessed compared with synchrotron-based measurements. Raman spectroscopy probes the phonon modes of the materials. The sp^2 bonds in the classic honeycomb structural units of various sp^2-bonded carbon materials are known to have strong Raman signatures. However, analytical results currently show a high level of discreteness, and there is no one consistent conclusion about the specific evolution of C−C bonds under high-pressure conditions. Moreover, it is not clear whether different types of sp^2-bonded carbon precursors will experience a similar process or a distinct process of high-pressure-induced chemical bond change. In this work, micro-Raman spectroscopy is used to track *in situ* the evolution of C−C bonds in three sp^2-bonded carbon precursors with a range of different microstructures covering glassy carbon, highly crystalline natural graphite, and multiwall carbon nanotubes. The specific changes in the *in situ* Raman spectrum are systematically collected and carefully analyzed for the three carbon precursors during their loading and unloading of up to 54 GPa.

Three types of carbon precursors are all mainly sp^2-bonded, have layerlike structures, and are of interest as high-pressure precursors for novel carbon phase formation. Glassy carbon (GC, Sigradur-G-3000, HTW Hochtemperatur-Werkstoffe GmbH) is composed of turbostatic graphitic layers and has more than 95% sp^2 C−C bonds.[32,33] Highly crystalline natural graphite was purchased from the Graphene Supermarket Corp. It has a purity of up to 99.75% and consists of hexagonal regular layer structures. Multiwall carbon nanotubes (MWCNTs) from Merck were also analyzed. These MWCNTs are made of multiple concentric single-walled carbon nanotubes through van der Waals interactions. They will be flattened under high-pressure conditions and thus are intrinsically similar to graphitic structures due to severe compression. All three carbon precursors were used without any other treatments like annealing.

High-pressure experiments were carried out using an Almax plate diamond anvil cell (DAC) with 250 μm culets. Stainless steel gaskets with a thickness of ~300 μm and a diameter of ~1300 μm were preindented and then drilled using a Boehler microDriller to make a specimen chamber with a diameter of ~100 μm and a thickness of ~40 μm. GC, graphite, and MWCNTs were individually loaded into specimen chambers in the center of gaskets without any pressure-transmitting medium to potentially generate a large shear force for samples under high-pressure conditions. The applied pressure was measured through the pressure-dependent shift of the Raman peak of the diamond anvils.[34]

Raman spectra of samples were all measured *in situ* using a Renishaw *InVia* micro-Raman spectrometer equipped with a 532 nm laser and a long working distance objective of 20×. Raman data were collected *in situ* under both loading and unloading. The collected Raman spectra were fitted using a Lorentzian function using Fityk.[35] Considering the potential errors from pressure tests and calibration (±1 GPa) and possible uncertainties during peak fitting (±3 cm^{-1}), error bars are added to our Raman data. It should be noted that the diamond anvil itself generates a strong diamond Raman band from 1332 to 1450 cm^{-1} in the pressure range of ambient to 54 GPa. This diamond peak overlaps with the disorder peak of sp^2-bonded carbon precursors but is well separated from the graphite peak (G peak) under high pressure.

Figure 1 shows Raman spectra of GC, graphite, and MWCNTs under ambient conditions before pressure treatment. GC has a strong disorder (D peak) at ~1348 cm^{-1} and a broad G peak centered around 1589 cm^{-1}. The D peak comes from the TO phonon mode near K points in the Brillouin zone and strongly correlates with the disordered structure of GC.[36,37] It overlaps with the diamond Raman peak of diamond anvils under high-pressure conditions. The G peak originates from the double-degenerate zone-center E_{2g} phonon mode[36] and corresponds to intralayer C−C stretching vibrations. It intrinsically represents the pressure-dependent changes in C−C bonds in a honeycomb structure. A tiny shoulder D* peak is observed on the high-frequency side of the G peak, and it could be attributed to an additional disorder-related peak from the intravalley double resonance.[37] The second-order Raman scattering 2D and D+G peaks of GC are detected at ~2688 and ~2939 cm^{-1}, respectively. Graphite presents a sharp and narrow G peak and a very weak D peak due to its high crystallinity. The 2D peak of graphite is split into two Raman peaks (2D and 2D′) at 2686 and 2720 cm^{-1}, while its D+G peak cannot be detected. MWCNTs display a Raman spectrum similar to that of GC, but it has less disorder or fewer defects given a higher ratio of the G to D peak in contrast to that of GC.

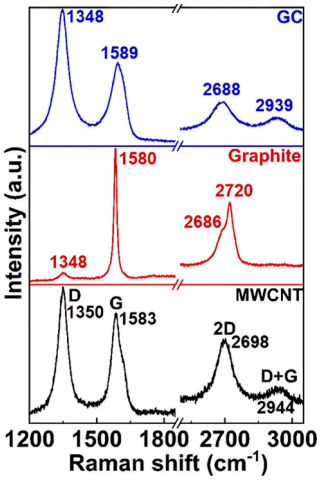

Figure 1. Raman spectra of glassy carbon (GC), graphite, and multiwall carbon nanotubes (MWCNT) collected under ambient conditions.

As shown in Figure 2a, the G peak of GC becomes broader and shifts to a higher frequency under pressurization. The peak position shifts from ~1589 to ~1685 cm^{-1} (at ~52 GPa), a change of ~96 cm^{-1}. This indicates that the intralayer C−C bond length is shortened due to the high-pressure

https://doi.org/10.1021/acs.jpclett.5c01578
J. Phys. Chem. Lett. XXXX, XXX, XXX−XXX

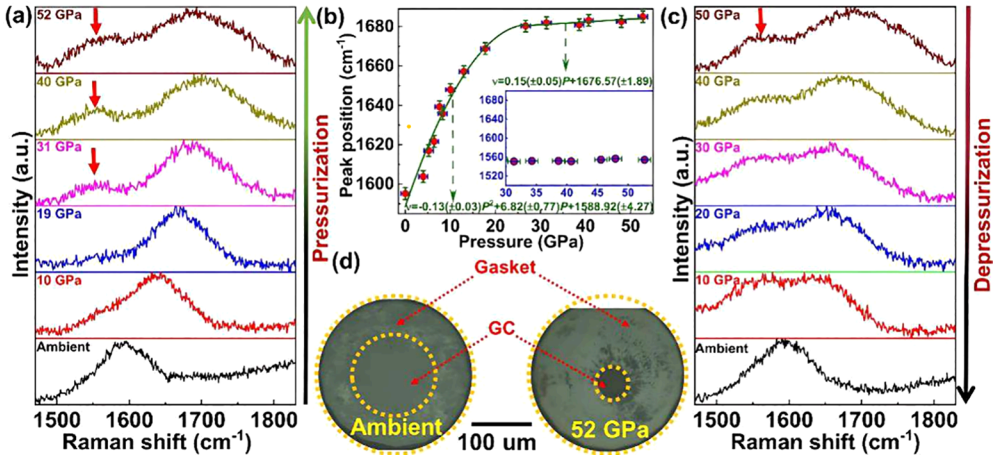

Figure 2. *In situ* Raman spectra of glassy carbon collected in the pressure range from ambient to ~52 GPa under (a) pressurization and (c) depressurization. Red arrows here mark the Raman peaks of C−C interlinkage bonds in GC. (b) Pressure-dependent G peak positions and associated fitting curves using a polynomial and linear function. The inset of panel b shows the peak position of the new peak from C−C interlinkage bonds as a function of pressure. (d) Optical photographs taken using both transmission and reflection light illumination.

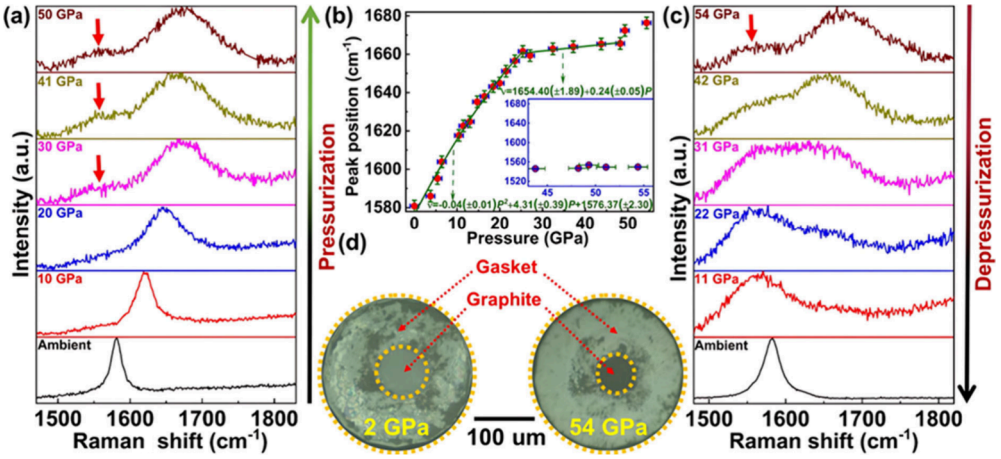

Figure 3. Raman spectra of highly crystalline natural graphite collected from ambient to 54 GPa under (a) *in situ* pressurization and (c) depressurization. Red arrows label the Raman peaks of C−C interlinkage bonds in graphite. (b) Pressure vs G peak position and associated fitting curves employing a polynomial and linear function. The inset of panel b shows the peak position of the new peak attributed to C−C interlinkage peaks as a function of pressure. (d) Optical photographs of graphite taken using both transmission and reflection visible light illumination.

compression. When the G peak positions of GC are fitted through the Lorentzian function (the detailed fitting process can be found in the Supporting Information) and plotted as a function of associated pressure (Figure 2b), it is found that the G peak shifting of GC can be divided into two stages. In stage 1 from ambient to ~30 GPa, the G peak of GC migrates following a polynomial curve with a first-order pressure coefficient of about 6.82 ± 0.77 cm^{-1} GPa^{-1} ($d\nu/dp$, where ν is the Raman shift in cm^{-1} and p is the pressure in GPa) and the second-order coefficient $[(d\nu)^2/(dp)^2]$ of −0.13 ± 0.03 cm^{-2} GPa^{-2}. In stage 2 from ~30 to ~52 GPa, the G peak sluggishly moves following a linear function with a $d\nu/dp$ value of 0.15 cm^{-1} GPa^{-1}. At the maximum pressure of ~52 GPa, GC is still as opaque as that under ambient conditions (see the optical images in Figure 2d).

It is interesting to note that a new broad Raman peak at ~1554 cm^{-1} appears in the Raman spectra collected between ~30 and ~52 GPa (Figure 2a). This new peak becomes more visible at higher pressures such as ~40 and ~52 GPa. The new peak coincides with the transition to stage 2 of the G peak movement. Interestingly, this peak does not significantly shift over the pressure range of 30−50 GPa (inset of Figure 2b). The formation of this new peak perhaps leads to a dramatic change in the shift of the G peak as a function of pressure. The new peak at ~1554 cm^{-1} disappears at a higher pressure like ~80 GPa (it will be reported in another paper). It is a characteristic Raman peak of CCIBs (i.e., carbon atoms in two neighboring layers interlink together under high-pressure conditions). The detailed discussion about CCIBs is as follows. The generation of this new CCIB peak perhaps leads to the abnormal change in G peak movement from stage 1 to stage 2 and its subsequent sluggish migration at the latter since it consumes the most energy (i.e., pressure here).

When the pressure is released, the peak position of CCIBs does not appear to move with a decrease in pressure to ~10 GPa but is not observed under ambient conditions (Figure 2c), suggesting that the CCIBs generated on loading between ~30 and ~52 GPa are metastable and reversible. This is different from the G peak of GC that gradually moves back to its initial position when the pressure is released.

To investigate whether the change in the shift of the G peak and the generation of the CCIB peak observed in GC also

https://doi.org/10.1021/acs.jpclett.5c01578
J. Phys. Chem. Lett. XXXX, XXX, XXX−XXX

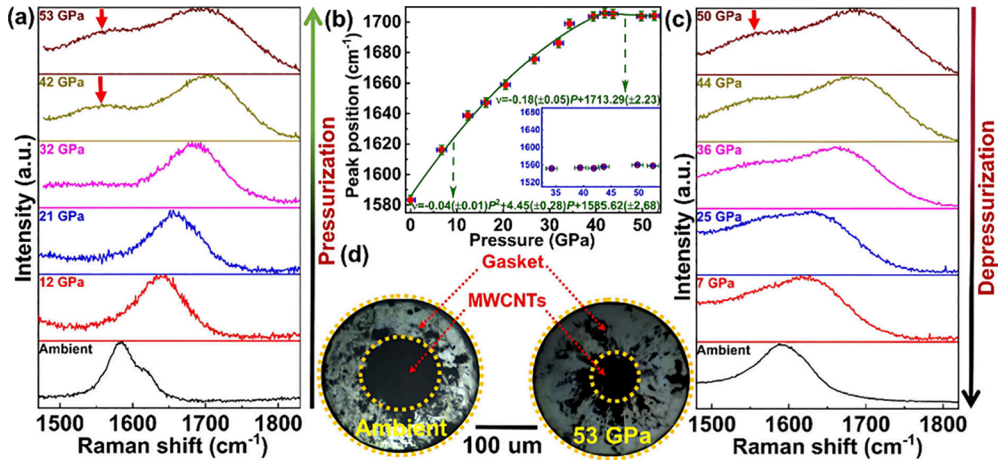

Figure 4. *In situ* Raman spectra of multiwall carbon nanotubes (MWCNTs) collected from ambient to 53 GPa under (a) pressurization and (c) depressurization. Raman peaks of C−C interlinkage bonds in MWCNTs are marked by red arrows. (b) Pressure vs G peak position of MWCNTs and associated fitting curves employing a polynomial and linear function. The inset of panel b shows the peak position of a new peak attributed to C−C interlinkage peaks as a function of pressure. (d) Optical photographs of MWCNTs taken using both transmission and reflection visible light illumination.

Table 1. Summary of the Experimental Conditions, Pressure Ranges, and Pressure Coefficients (E_{2g} Raman mode) Reported for Carbon Materials in the Literature and by Us[a]

					stage 1			stage 2		
sample	DAC (culet size)	calibration	PTM	gasket	pressure (GPa)	$d\nu/dp$ (cm^{-1} GPa^{-1})	$(d\nu)^2/(dp)^2$ (cm^{-2} GPa^{-2})	pressure (GPa)	$d\nu/dp$ (cm^{-1} GPa^{-1})	ref
GC	P250	diamond	none	steel	<30	6.82	−0.13	30−52	0.15	this work
graphite	P250	diamond	none	steel	<27	4.31	−0.04	25−54	0.24	this work
graphite	Pa300	ruby	Ne	Re (80 μm)	UKN	4.24	−0.02	–	–	27
graphite	Pa300	ruby	NaCl	Re (80 μm)	<30	4.32	−0.04	30−80	0.41	27
graphite	UKN300	ruby	MeOH and EtOH	Re (50 μm)	<30	4.32	−0.04	–	–	31
graphite	UKN	ruby	MeOH and EtOH	UKN	<14	4.7	UKN	–	–	29
graphite	UKN300/400	ruby	Ne	UKN	<54	3.6	−0.02	–	–	41
GNP	UKN300/400	ruby	He	UKN	<53	4.02	−0.03	–	–	41
GNP	UKN300/400	ruby	Ar	UKN	<53	4.49	−0.04	–	–	41
MWCNTs	P-250	diamond	none	steel	<42	4.45	−0.04	42−53	−0.18	this work

[a]Abbreviations: DACs, diamond anvil cells; GC, glassy carbon; graphite; GNP, graphene nanoplatelet; MWCNTs, multiwall carbon nanotubes; PTM, pressure-transmitting medium; P in DAC column, plate DAC; Pa in DAC column, panoramic DAC; UKN, unknown.

happen in other carbon materials, graphite was also compressed in plate DACs to 54 GPa (a pressure close to that of GC). Surprisingly, the G peak of graphite is found to present a similar change as that of GC under high pressure. It gradually moves to high frequencies and becomes broad under compression as shown in Figure 3a. The pressure-dependent G peak shift of graphite is also composed of two separate stages (Figure 3b), that is, a polynomial movement from ∼1580 cm^{-1} (ambient) to 1660 cm^{-1} (∼25 GPa) in stage 1 and a nearly linear shift from ∼1660 to 1676 cm^{-1} (∼54 GPa) in stage 2. The first and second pressure coefficients in stage 1 are 4.31 ± 0.39 cm^{-1} GPa^{-1} and −0.04 ± 0.01 cm^{-2} GPa^{-2}, respectively. The pressure coefficient in stage 2 is about 0.24 ± 0.05 cm^{-1} GPa^{-1}. At a maximum pressure of ∼54 GPa, graphite is also not optically transparent (Figure 3d). It should be pointed out that the new Raman peak of CCIBs is also detected in graphite above ∼30 GPa. Furthermore, the peak position of CCIBs is at ∼1550 cm^{-1} and is also very close to that of the GC (Figure 2a). When the pressure is released, this CCIB peak does not move with a decrease in pressure and finally disappears under ambient conditions (Figure 3c). The G peak of graphite recovers to its initial position but becomes slightly broader. It is thus demonstrated that pressure-induced G peak migration has two stages and CCIBs are formed under high-pressure conditions, again.

Given common phenomena are observed in the *in situ* Raman spectra of GC and graphite, it is interesting to explore if another sp^2-bonded carbon precursor exhibits a similar behavior under high pressure. MWCNTs, which have a layer structure with sp^2 C−C bonds, are subsequently pressurized to about 53 GPa. One can see that the G peak of MWCNTs shifts from ∼1583 cm^{-1} (ambient) to ∼1700 cm^{-1} (∼41 GPa) (Figure 4a) and also presents a two-stage movement (Figure 4b). The first and second pressure coefficients of the sublinear curve in stage 1 are 4.45 ± 0.28 and −0.04 ± 0.01 cm^{-1} GPa^{-1}, respectively. The two values are close to that of graphite

https://doi.org/10.1021/acs.jpclett.5c01578
J. Phys. Chem. Lett. XXXX, XXX, XXX−XXX

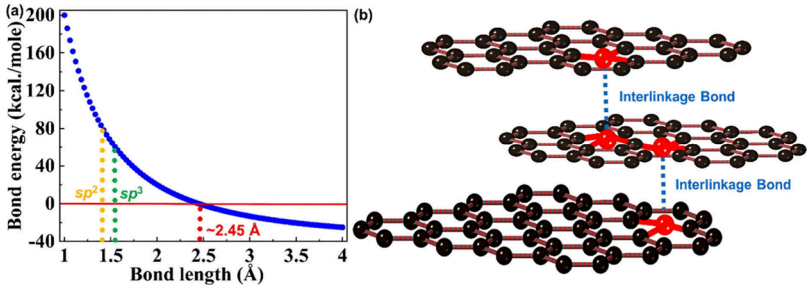

Figure 5. (a) Binding energy vs bond length of a carbon−carbon single bond. (b) Atomic motif depicting carbon−carbon interlinkage bonds formed under high-pressure conditions.

(Figure 3b). Further increasing the pressure nearly does not change the position of the G peak and leads to a pressure coefficient of -0.18 ± 0.05 cm^{-1} GPa^{-1} in stage 2. The new Raman peak at ~1550 cm^{-1} is also found in MWCNTs (e.g., Raman spectra collected at ~42 and ~53 GPa). It stands still with increasing pressures as that of GC and graphite (inset of Figure 4b). Under decompression, the CCIB peak does not alter its position and completely disappears under ambient conditions (Figure 4c). Meanwhile, the G peak gradually shifts to its initial position and also becomes broader, which is similar to the case for graphite. MWCNTs do not become transparent even though they are compressed to ~53 GPa (Figure 4d).

Through *in situ* Raman spectra of GC, graphite,and MWCNTs, one solid conclusion regarding the high-pressure-induced two-stage shift of the G peak can be reached for the three different types of sp^2-bonded carbon precursors. The two-stage movement of the G peak was also observed by other researchers in their compression of graphite,[27,38] glassy carbon,[18] and MWCNTs.[38,39] Table 1 summarizes our experimental conditions, pressure ranges, and pressure coefficients of the E_{2g} Raman mode. Experimental data taken from the literature are also listed here. The critical pressure for the transition from stage 1 to stage 2 measured here is also close to that reported in the literature, i.e., about 30 GPa for graphite and glassy carbon and about 40 GPa for MWCNTs. Although the exact reason why MWCNTs have a higher critical pressure is unclear, it is possibly related to their larger bulk modulus of a few hundred gigapascals in contrast to that of 38 GPa for GC[40] and 34 GPa for graphite.[29] The change of the G peak shift indicates a possible beginning of a structural transition[39] or bonding of interlayer carbon atoms in carbon precursors. In the following stage 2, we indeed observe the softening of the E_{2g} Raman mode (i.e., the peak position of the Raman mode does not change with pressure) and the generation of one new Raman peak at about 1550 cm^{-1}.

It should be pointed out that the polynomial migration of the G peak in stage 1 has also been previously reported.[27,29,31,38,39,41] This movement could not be attributed to the rehybridization of carbon atoms from π-bonds to σ-bonds[27] since the interlayer distance in the pressure range of stage 1 is more than 2.8 Å.[15,17,21,22] Such a long distance makes it difficult to form σ-bonds through binding interlayer carbon atoms (the details are shown in Figure 5). The polynomial shift highly possibly originates in the strong anisotropy of local and average structures in these layer-like carbon precursors. We further find that the unit cell volume of these carbon materials follows a polynomial change under high-pressure conditions.[17,42,43] Based on the relationship of the pressure-dependent Raman frequency and unit cell volume, $\frac{\nu_p}{\nu_0} = \left(\frac{V_p}{V_0}\right)^{-\gamma_G}$ (where ν_p, ν_0, V_p, and V_0 are the E_{2g} Raman frequency and unit cell volume of sp^2-bonded carbon materials at ambient and variable pressure, respectively, and γ_G is the mode Grüneisen parameter and a constant),[29] the sublinear shrinkage of the unit cell volume would inevitably lead to the same shift trend of the Raman peaks. More interestingly, the polynomial movement of Raman modes under high pressure was also observed in other layered materials with strong structural anisotropy, including 2*H*-MoX_2 (X = S, Se, and Te),[44] $Ti_3C_2T_x$ MXene,[45] and $Mo_{0.5}W_{0.5}S_2$ ternary compounds.[46] It thus seems that the polynomial shift of Raman peaks prior to the pressure-induced phase transition and chemical reaction should be a common feature of layered materials. It should also be pointed out that a larger first-order pressure coefficient of 6.82 cm^{-1} GPa^{-1} is observed for GC and is much larger than that of graphite (4.31 cm^{-1} GPa^{-1}). Such a large deviation could be attributable to a lower volumetric density (that of GC is about 1.5 g/cm^3, and that of graphite is about 2.26 g/cm^3).[33,47]

We now discuss the possible origin of the new Raman peak observed at about 1550 cm^{-1} and in the stage 2 shift of the G peak and why it can be detected under high-pressure conditions. We find that the 1550 cm^{-1} Raman peak appears in other high-pressure experiments during the compression of graphite[27,28,48] and glassy carbon.[28,49] This peak is also usually detected in tetrahedral amorphous carbon[50−52] and bundled single-wall carbon nanotubes[53,54] under ambient conditions. It could be attributed to many possible reasons such as the fluorescence and contamination from diamond anvils, the visibility of the F band, the splitting of the G peak, the generation of new carbon structures, and the formation of C−C interlinkage bonds.

Diamond mounted in our DACs exhibits ultralow fluorescence. There is no visible fluorescence peak at about 1550 cm^{-1} in the Raman spectra collected at a lower pressure such as 10 or 20 GPa (Figures 2−4). Even if the intensity of diamond fluorescence is dependent on pressure, it is normally detected above 100 GPa and disappears at 280 GPa, relying on specific diamond, the frequency of excitation, and the window of detection.[55] Our pressure is much lower than that of diamond to activate fluorescence. Furthermore, the new 1550 cm^{-1} Raman peak is not detected in our experiments of compressing some other materials such as oxides and hydroxides when the same diamond anvil cells are used. Therefore, the Raman peak at about 1550 cm^{-1} should not be related to the diamond fluorescence of DACs.

This new Raman peak could not originate from the F band as observed in the pressurization of glassy carbon micro-

https://doi.org/10.1021/acs.jpclett.5c01578
J. Phys. Chem. Lett. XXXX, XXX, XXX−XXX

balls.[16,30] We note that the Raman peak of the F band arises at about 1420 cm^{-1} and linearly shifts to about 1620 cm^{-1} at ∼60 GPa. Such a large shift of about 200 cm^{-1} should be clearly observed in our experiments if it also exists here. Actually, the peak positions of the new Raman bands of GC, graphite, and MWCNTs are all unchanged under high-pressure conditions (insets of Figures 2b−4b). In addition, the merging of the F and G bands above 45 GPa leads to the downshifting of the G peak. This phenomenon is also not seen in our Raman spectra. The strain-driven splitting of the G peak[56] could be also responsible for the origin of the new 1550 cm^{-1} Raman peak. However, we carefully checked our Raman spectra and did not find any clue about G peak splitting in the pressure range of up to 54 GPa. More importantly, two Raman peaks spilt from the G peak both red-shift with an increase in strain, and the separation between the new peak and the G band should increase with pressure. These phenomena are inconsistent with our observation here.

Another possibility of generating a new 1550 cm^{-1} Raman peak is related to the formation of new carbon structures. *In situ* synchrotron X-ray diffraction patterns of sp^2-bonded carbon materials like GC have been measured in our pressure range.[14,15,17,21,22,42,43] The average interlayer distance shortens to about 2.4−2.7 Å with an increase in pressure to ∼50 GPa; the C−C−C bond angle remains at ∼120° of a honeycomb structure, and the coordination number of carbon atoms is close to 3.[15] No clear evidence shows that an sp^3 structure can be synthesized below 54 GPa. In further combination of theoretical calculation and simulation,[7,57−59] a high pressure of up to 70−80 GPa is required to form permanent interlayer sp^3 bonds. Most sp^3 allotropes (e.g., monoclinic, body-centered tetragonal, and orthorhombic carbon) do not present one nonshifted Raman band at around 1550 cm^{-1} between 30 and 50 GPa. This solid structural information and theoretical support make us believe that the new Raman peak observed in the pressurization of GC, graphite, and MWCNTs does not originate in a new sp^3 carbon phase.

In order to further understand the origin of this new Raman peak at about 1550 cm^{-1}, the binding energy (E) of a C−C single bond at variable bond lengths (R) is calculated based on the formula $E = 240/R^2 - 40$.[60] It is plotted in Figure 5a. Under ambient conditions, interlayer carbon atoms could have a distance of 3.35 Å (e.g., graphite and MWCNTs) and interact with each other through van der Waals force. At this long distance, the interaction of interlayer carbon atoms nearly does not contribute to phonon vibrations and thus is not considered in conventional phonon mode calculations. However, high pressure will seriously shorten the interlayer distance of sp^2-bonded carbon materials to about 2.4−2.7 Å in the pressure range of 30−50 GPa.[15,17] The bond length to chemically bind two interlayer carbon atoms for forming CCIBs is about 2.45 Å, as shown in Figure 5a. It is reasonably consistent with the measurement results of synchrotron XRD. In this scenario, the contribution of CCIBs to phonon vibrations cannot be neglected and leads to the appearance of a new Raman band at 1550 cm^{-1} in the high-pressure Raman spectra of GC, graphite, and MWCNTs.

Figure 5b presents an atomic motif of CCIBs based on the experimental results of Raman spectroscopy and available structural data. Given that the bond of CCIBs is much longer than normal sp^2 bonds (∼1.42 Å), its Raman peak should appear at a much lower frequency than that of the G peak, which is consistent with our experimental results. The formation of CCIBs softens the E_{2g} phonon mode and thus keeps its Raman peak position between 30 and 54 GPa. In light of further E_{2g} Raman mode softening and the formation of CCIBs in this pressure range, both of their Raman peaks should not shift with a change in pressure. Additionally, it should be noted that the binding energy of CCIBs is rather low compared to that of C−C bonds in honeycomb structures of GC and graphite (∼82.5 kcal/mol) as well as those in tetrahedral units of diamonds (∼62.5 kcal/mol).[58] Meanwhile, the bond of CCIBs is also much longer than that of diamonds (1.54 Å), GC, and graphite. CCIBs thus would disappear once the pressure was released and present a metastable and reversible feature. The formation of CCIBs under high-pressure conditions can well interpret why a significant percentage of sp^3 bonds could not be discovered in carbon samples retrieved from 50 GPa and carbon materials like GC can only graphitize in such a pressure range.

In summary, carbon−carbon interlinkage bonds are discovered in the compression and decompression of multiple types of sp^2-bonded carbon precursors, including glassy carbon, graphite, and multiwall carbon nanotubes, using micro-Raman spectroscopy. These carbon−carbon interlinkage bonds have a metastable characteristic, maintain their peak position under high-pressure conditions, and completely disappear once the pressure is released. The G peak of all three precursors presents a similar two-stage (polynomial and linear) migration with an increase in pressure, but the first pressure coefficient of glassy carbon is much higher than those of the other two due to its softness. The formation of carbon−carbon interlinkage bonds leads to a two-stage shift of the G peak and is an intermediate step for the transition of sp^2 to sp^3 bonds. This discovery will benefit the synthesis of various sp^3-rich carbon structures and advances our understanding of the high-pressure-induced phase transition of carbon materials.

■ ASSOCIATED CONTENT

Supporting Information

The Supporting Information is available free of charge at https://pubs.acs.org/doi/10.1021/acs.jpclett.5c01578.

Fitting of Raman spectra (PDF)

■ AUTHOR INFORMATION

Corresponding Authors

Qingbo Sun − *Department of Materials Physics, Research School of Physics, The Australian National University, Canberra, Australian Capital Territory 2601, Australia;* orcid.org/0000-0003-3546-0018; Email: Qingbo.Sun@anu.edu.au

Jodie E. Bradby − *Department of Materials Physics, Research School of Physics, The Australian National University, Canberra, Australian Capital Territory 2601, Australia;* orcid.org/0000-0002-9560-8400; Email: Jodie.Bradby@anu.edu.au

Authors

Jian-Tao Wang − *Beijing National Laboratory for Condensed Matter Physics, Institute of Physics, Chinese Academy of Sciences, Beijing 100190, China; School of Physical Sciences, University of Chinese Academy of Sciences, Beijing 100049, China; Songshan Lake Materials Laboratory, Dongguan, Guangdong 523808, China;* orcid.org/0000-0002-0786-1212

https://doi.org/10.1021/acs.jpclett.5c01578
J. Phys. Chem. Lett. XXXX, XXX, XXX−XXX

Xingshuo Huang − *Department of Materials Physics, Research School of Physics, The Australian National University, Canberra, Australian Capital Territory 2601, Australia;* orcid.org/0000-0001-8491-5176

Guoyin Shen − *HPCAT, X-ray Science Division, Argonne National Laboratory, Argonne, Illinois 60439, United States;* orcid.org/0000-0001-5146-1147

Complete contact information is available at: https://pubs.acs.org/10.1021/acs.jpclett.5c01578

Notes

The authors declare no competing financial interest.

■ ACKNOWLEDGMENTS

J.E.B. and Q.S. acknowledge funding support from the Australian Research Council (ARC) through the ARC Discovery Project (DP190101438). J.-T.W. acknowledges support from the National Key Research and Development Program of China (Grant 2020YFA0711502), the National Natural Science Foundation of China (Grants 11674364, 11974387, 92263202, and 12374020), and the Strategic Priority Research Program of the Chinese Academy of Sciences (Grant XDB33000000).

■ REFERENCES

(1) Tang, H.; Yuan, X.; Cheng, Y.; Fei, H.; Liu, F.; Liang, T.; Zeng, Z.; Ishii, T.; Wang, M.-S.; Katsura, T.; Sheng, H.; Gou, H. Synthesis of paracrystalline diamond. *Nature* **2021**, *599*, 605−610.

(2) Shang, Y.; Liu, Z.; Dong, J.; Yao, M.; Yang, Z.; Li, Q.; Zhai, C.; Shen, F.; Hou, X.; Wang, L.; Zhang, N.; Zhang, W.; Fu, R.; Ji, J.; Zhang, X.; Lin, H.; Fei, Y.; Sundqvist, B.; Wang, W.; Liu, B. Ultrahard bulk amorphous carbon from collapsed fullerene. *Nature* **2021**, *599*, 599−604.

(3) Huang, Q.; Yu, D.; Xu, B.; Hu, W.; Ma, Y.; Wang, Y.; Zhao, Z.; Wen, B.; He, J.; Liu, Z.; Tian, Y. Nanotwinned diamond with unprecedented hardness and stability. *Nature* **2014**, *510*, 250−253.

(4) Cui, H.-J.; Sheng, X.-L.; Yan, Q.-B.; Zhu, Z.-G.; Zheng, Q.-R.; Su, G. Diamond polytypes under high pressure: a first-principles study. *Comput. Mater. Sci.* **2015**, *98*, 129−135.

(5) Irifune, T.; Kurio, A.; Sakamoto, S.; Inoue, T.; Sumiya, H. Ultrahard polycrystalline diamond from graphite. *Nature* **2003**, *421*, 599−600.

(6) McCulloch, D. G.; Wong, S.; Shiell, T. B.; Haberl, B.; Cook, B. A.; Huang, X.; Boehler, R.; McKenzie, D. R.; Bradby, J. E. Investigation of room temperature formation of the ultra-hard nanocarbons diamond and lonsdaleite. *Small* **2020**, *16*, 2004695.

(7) Dong, X.; Zhou, X.-F.; Qian, G.-R.; Zhao, Z.; Tian, Y.; Wang, H.-T. An *ab initio* study on the transition paths from graphite to diamond under pressure. *J. Phys.: Condens. Matter* **2013**, *25*, 145402.

(8) Fahy, S.; Louie, S. G.; Cohen, M. L. Pseudopotential total-energy study of the transition from rhombohedral graphite to diamond. *Phys. Rev. B* **1986**, *34*, 1191.

(9) Tateyama, Y.; Ogitsu, T.; Kusakabe, K.; Tsuneyuki, S. Constant-pressure first-principles studies on the transition states of the graphite-diamond transformation. *Phys. Rev. B* **1996**, *54*, 14994.

(10) Srinivasan, S.; Batra, R.; Luo, D.; Loeffler, T.; Manna, S.; Chan, H.; Yang, L.; Yang, W.; Wen, J.; Darancet, P.; Sankaranarayanan, S. K. R. S. Machine learning the metastable phase diagram of covalently bonded carbon. *Nat. Commun.* **2022**, *13*, 3251.

(11) Wong, S.; Shiell, T.; Cook, B.; Bradby, J.; McKenzie, D.; McCulloch, D. The shear-driven transformation mechanism from glassy carbon to hexagonal diamond. *Carbon* **2019**, *142*, 475−481.

(12) Shiell, T. B.; McCulloch, D. G.; Bradby, J. E.; Haberl, B.; Boehler, R.; McKenzie, D. R. Nanocrystalline hexagonal diamond formed from glassy carbon. *Sci. Rep.* **2016**, *6*, 37232.

(13) Shiell, T. B.; McCulloch, D. G.; McKenzie, D. R.; Field, M. R.; Haberl, B.; Boehler, R.; Cook, B. A.; de Tomas, C.; Suarez-Martinez, I.; Marks, N. A.; Bradby, J. E. Graphitization of Glassy Carbon after Compression at Room Temperature. *Phys. Rev. Lett.* **2018**, *120*, 215701.

(14) Shiell, T. B.; de Tomas, C.; McCulloch, D. G.; McKenzie, D. R.; Basu, A.; Suarez-Martinez, I.; Marks, N. A.; Boehler, R.; Haberl, B.; Bradby, J. E. *In situ* analysis of the structural transformation of glassy carbon under compression at room temperature. *Phys. Rev. B* **2019**, *99*, No. 024114.

(15) Shibazaki, Y.; Kono, Y.; Shen, G. Compressed glassy carbon maintaining graphite-like structure with linkage formation between graphene layers. *Sci. Rep.* **2019**, *9*, 7531.

(16) Solopova, N. A.; Dubrovinskaia, N.; Dubrovinsky, L. Raman spectroscopy of glassy carbon up to 60 GPa. *Appl. Phys. Lett.* **2013**, *102*, 121909.

(17) Tan, L.; Sheng, H.; Lou, H.; Cheng, B.; Xuan, Y.; Prakapenka, V. B.; Greenberg, E.; Zeng, Q.; Peng, F.; Zeng, Z. High-pressure tetrahedral amorphous carbon synthesized by compressing glassy carbon at room temperature. *J. Phys. Chem. C* **2020**, *124*, 5489−5494.

(18) Yao, M.; Xiao, J.; Fan, X.; Liu, R.; Liu, B. Transparent, superhard amorphous carbon phase from compressing glassy carbon. *Appl. Phys. Lett.* **2014**, *104*, No. 021916.

(19) Solopova, N. A.; Dubrovinskaia, N.; Dubrovinsky, L. Synthesis of nanocrystalline diamond from glassy carbon balls. *J. Cry. Growth* **2015**, *412*, 54−59.

(20) Mao, W. L.; Mao, H.-K.; Eng, P. J.; Trainor, T. P.; Newville, M.; Kao, C.-C.; Heinz, D. L.; Shu, J.; Meng, Y.; Hemley, R. J. Bonding changes in compressed superhard graphite. *Science* **2003**, *302*, 425−427.

(21) Zeng, Z.; Sheng, H.; Yang, L.; Lou, H.; Tan, L.; Prakapenka, V. B.; Greenberg, E.; Zeng, Q. Structural transition in cold-compressed glassy carbon. *Phys. Rev. Mater.* **2019**, *3*, No. 033608.

(22) Lin, Y.; Zhang, L.; Mao, H.-K.; Chow, P.; Xiao, Y.; Baldini, M.; Shu, J.; Mao, W. L. Amorphous diamond: a high-pressure superhard carbon allotrope. *Phys. Rev. Lett.* **2011**, *107*, 175504.

(23) Yagi, T.; Utsumi, W.; Yamakata, M.-A.; Kikegawa, T.; Shimomura, O. High-pressure *in situ* x-ray-diffraction study of the phase transformation from graphite to hexagonal diamond at room temperature. *Phys. Rev. B* **1992**, *46* (10), 6031.

(24) Hu, M.; He, J.; Zhao, Z.; Strobel, T. A.; Hu, W.; Yu, D.; Sun, H.; Liu, L.; Li, Z.; Ma, M.; Kono, Y.; Shu, J.; Mao, H.-K.; Fei, Y.; Shen, G.; Wang, Y.; Juhl, S. J.; Huang, J. Y.; Liu, Z.; Xu, B.; Tian, Y. Compressed glassy carbon: an ultrastrong and elastic interpenetrating graphene network. *Sci. Adv.* **2017**, *3*, No. e1603213.

(25) Scandolo, S.; Bernasconi, M.; Chiarotti, G. L.; Focher, P.; Tosatti, E. Pressure-induced transformation path of graphite to diamond. *Phys. Rev. Lett.* **1995**, *74* (20), 4015−4018.

(26) Khaliullin, R. Z.; Eshet, H.; Kühne, T. D.; Behler, J.; Parrinello, M. Nucleation mechanism for the direct graphite-to-diamond phase transition. *Nat. Mater.* **2011**, *10*, 693−697.

(27) Odake, S.; Zinin, P. V.; Hellebrand, E.; Prakapenka, V.; Liu, Y.; Hong, S.; Burgess, K.; Ming, L.-C. Formation of the high pressure graphite and BC_8 phases in a cold compression experiment by Raman scattering. *J. Raman Spectrosc.* **2013**, *44*, 1596−1602.

(28) Goncharov, A. F. Graphite at high pressures: amorphization at 44 GPa. *Inter. J. High Press. Res.* **1992**, *8* (4), 607−616.

(29) Hanfland, M.; Beister, H.; Syassen, K. Graphite under pressure: equation of state and first-order Raman modes. *Phys. Rev. B* **1989**, *39* (7), 12598.

(30) Yao, M.; Xiao, J.; Fan, X.; Liu, R.; Liu, B. Transparent, superhard amorphous carbon phase from compressing glassy carbon. *Appl. Phys. Lett.* **2014**, *104*, No. 021916.

(31) Schindler, L.; Vohra, Y. K. A micro-Raman investigation of high-pressure quenched graphite. *J. Phys.: Condens. Matter* **1995**, *7*, L637.

(32) Jurkiewicz, K.; Pawlyta, M.; Zygadło, D.; Chrobak, D.; Duber, S.; Wrzalik, R.; Ratuszna, A.; Burian, A. Evolution of glassy carbon

under heat treatment: correlation structure-mechanical properties. *J. Mater. Sci.* **2018**, *53*, 3509−3523.
(33) Shiell, T. B.; Wong, S.; Yang, W.; Tanner, C. A.; Haberl, B.; Elliman, R. G.; McKenzie, D. R.; McCulloch, D. G.; Bradby, J. E. The composition, structure and properties of four different glassy carbons. *J. Non-Cryst. Solids* **2019**, *522*, 119561.
(34) Akahama, Y.; Kawamura, H. Pressure calibration of diamond anvil Raman gauge to 310 GPa. *J. Appl. Phys.* **2006**, *100*, No. 043516.
(35) Wojdyr, M. *Fityk*: a general-purpose peak fitting program. *J. Appl. Crystallogr.* **2010**, *43*, 1126−1128.
(36) Ferrari, A. C.; Meyer, J. C.; Scardaci, V.; Casiraghi, C.; Lazzeri, M.; Mauri, F.; Piscanec, S.; Jiang, D.; Novoselov, K. S.; Roth, S.; Geim, A. K. Raman spectrum of graphene and graphene layers. *Phys. Rev. Lett.* **2006**, *97*, 187401.
(37) Hong, J.; Park, M. K.; Lee, E. J.; Lee, D.; Hwang, D. S.; Ryu, S. Origin of new broad Raman D and G peaks in annealed graphene. *Sci. Rep.* **2013**, *3*, 2700.
(38) Blank, V. D.; Churkin, V. D.; Kulnitskiy, B. A.; Perezhogin, I. A.; Kirichenko, A. N.; Erohin, S. V.; Sorokin, P. B.; Popov, M. Y. Pressure-induced transformation of graphite and diamond to onions. *Crystals* **2018**, *8*, 68.
(39) Pashkin, E. Y.; Pankov, A. M.; Kulnitskiy, B. A.; Perezhogin, I. A.; Karaeva, A. R.; Mordkovich, V. Z.; Popov, M. Y.; Sorokin, P. B.; Blank, V. D. The unexpected stability of multiwall nanotubes under high pressure and shear deformation. *Appl. Phys. Lett.* **2016**, *109*, No. 081904.
(40) Wang, X.; Bao, Z. X.; Zhang, Y. L.; Li, F. Y.; Yu, R. C.; Jin, C. Q. High pressure effect on structural and electrical properties of glassy carbon. *J. Appl. Phys.* **2003**, *93*, 1991−1994.
(41) Efthimiopoulos, I.; Stavrou, E.; Umemoto, K.; Mayanna, S.; Torode, A.; Smith, J. S.; Chariton, S.; Prakapenka, V. B.; Goncharov, A. F.; Wang, Y. High-pressure phase of cold-compressed bulk graphite and graphene nanoplatelets. *Phys. Rev. B* **2023**, *107*, 184102.
(42) Zhao, Z.; Wang, E. F.; Yan, H.; Kono, Y.; Wen, B.; Bai, L.; Shi, F.; Zhang, J.; Kenney-Benson, C.; Park, C.; Wang, Y.; Shen, G. Nanoarchitectured materials composed of fullerene-like spheroids and disordered graphene layers with tunable mechanical properties. *Nat. Commun.* **2015**, *6*, 6212.
(43) Zeng, Z.; Yang, L.; Zeng, Q.; Lou, H.; Sheng, H.; Wen, J.; Miller, D. J.; Meng, Y.; Yang, W.; Mao, W. L.; Mao, H.-K. Synthesis of quenchable amorphous diamond. *Nat. Commun.* **2017**, *8*, 322.
(44) Sugai, S.; Ueda, T. High-pressure Raman spectroscopy in the layered materials 2*H*-MoS_2, 2*H*-$MoSe_2$, and 2*H*-$MoTe_2$. *Phys. Rev. B* **1982**, *26* (12), 6554−6558.
(45) Zhang, L.; Su, W.; Huang, Y.; Li, H.; Fu, L.; Song, K.; Huang, X.; Yu, J.; Lin, C.-T. *In situ* high-pressure X-ray diffraction and Raman spectroscopy study of $Ti_3C_2T_x$ MXene. *Nanoscale Res. Lett.* **2018**, *13*, 343.
(46) Kim, J.-S.; Moran, S. T.; Nayak, A. P.; Pedahzur, S.; Ruiz, I.; Ponce, G.; Rodriguez, D.; Henny, J.; Liu, J.; Lin, J.-F.; Akinwande, D. High pressure Raman study of layered $Mo_{0.5}W_{0.5}S_2$ ternary compound. *2D Mater.* **2016**, *3*, No. 025003.
(47) Savvatimskiy, A. I. Measurements of the melting point of graphite and the properties of liquid carbon (a review for 1963−2003). *Carbon* **2005**, *43*, 1115−1142.
(48) Wang, Y.; Panzik, J. E.; Kiefer, B.; Lee, K. K. M. Crystal structure of graphite under room-temperature compression and decompression. *Sci. Rep.* **2012**, *2*, 520.
(49) Goncharov, A. F.; Andreev, V. D. Raman scattering in carbon films at high pressures. *Sov. Phys. JETP* **1991**, *73* (1), 140−142.
(50) Gilkes, K. W. R.; Sands, H. S.; Batchelder, D. N.; Robertson, J.; Milne, W. I. Direct observation of bonding in tetrahedral amorphous carbon using ultraviolet Raman spectroscopy ***Appl.*** *Phys. Lett.* **1997**, *70*, 1980.
(51) Tamor, M. A.; Vassell, W. C. Raman "fingerprinting" of amorphous carbon films. *J. Appl. Phys.* **1994**, *76*, 3823.
(52) Chen, Z. Y.; Zhao, J. P.; Yano, T.; Ooie, T.; Yoneda, M.; Sakakibara, J. Observation of bonding in tetrahedral amorphous carbon using visible Raman spectroscopy. *J. Appl. Phys.* **2000**, *88*, 2305.
(53) Li, H. D.; Yue, K. T.; Lian, Z. L.; Zhan, Y.; Zhou, L. X.; Zhang, S. L.; Shi, Z. J.; Gu, Z. N.; Liu, B. B.; Yang, R. S.; Yang, H. B.; Zou, G. T.; Zhang, Y.; Iijima, S. Temperature dependence of the Raman spectra of single-wall carbon nanotubes. *Appl. Phys. Lett.* **2000**, *76*, 2053.
(54) Yu, Z.; Brus, L. Rayleigh and Raman scattering from individual carbon nanotube bundles. *J. Phys. Chem. B* **2001**, *105*, 1123−1134.
(55) Xu, J. A.; Mao, H. K.; Bell, P. M. High-pressure ruby and diamond fluorescence: observations at 0.21 to 0.55 terapascal. *Science* **1986**, *232* (4756), 1404−1406.
(56) Mohiuddin, T. M. G.; Lombardo, A.; Nair, R. R.; Bonetti, A.; Savini, G.; Jalil, R.; Bonini, N.; Basko, D. M.; Galiotis, C.; Marzari, N.; Novoselov, K. S.; Geim, A. K.; Ferrari, A. C. Uniaxial strain in graphene by Raman spectroscopy: G peak splitting, Grüneisen parameters, and sample orientation. *Phys. Rev. B* **2009**, *79*, 205433.
(57) Guo, W.; Zhu, C. Z.; Yu, T. X.; Woo, C. H.; Zhang, B.; Dai, Y. T. Formation of sp^3 bonding in nanoindented carbon nanotubes and graphite. *Phys. Rev. Lett.* **2004**, *93*, 245502.
(58) Flores-Livas, J. A.; Lehtovaara, L.; Amsler, M.; Goedecker, S.; Pailhès, S.; Botti, S.; San Miguel, A.; Marques, M. A. L. Raman activity of sp^3 carbon allotropes under pressure: a density functional theory study. *Phys. Rev. B* **2012**, *85*, 155428.
(59) Bai, Y.; Zhao, X.; Li, T.; Lv, Z.; Lv, S.; Han, H.; Yin, Y.; Wang, H. First-principles investigation in the Raman and infrared spectra of sp^3 carbon allotropes. *Carbon* **2014**, *78*, 70−78.
(60) Gordy, W. Dependence of bond order and of bond energy upon bond length. *J. Chem. Phys.* **1947**, *15* (5), 305−310.

https://doi.org/10.1021/acs.jpclett.5c01578
J. Phys. Chem. Lett. XXXX, XXX, XXX−XXX